Local protein kinase A action proceeds through intact holoenzymes

F. Donelson Smith[1], Jessica L. Esseltine[1†], Patrick J. Nygren[1], David Veesler[3], Dominic P. Byrne[2], Matthias Vonderach[2], Ilya Strashnov[4], Claire E. Eyers[2], Patrick A. Eyers[2], Lorene K. Langeberg[1] and John D. Scott[1*]

Affiliations:

[1]Howard Hughes Medical Institute, Department of Pharmacology, University of Washington, Seattle, WA 98195.

[2]Department of Biochemistry, Institute of Integrative Biology, University of Liverpool, Liverpool L69 7ZB, UK.

[3]Department of Biochemistry, University of Washington, Seattle, WA 98195.

[4]School of Chemistry, The University of Manchester, Manchester, M13 9PL, UK.

*Correspondence to: scottjdw@uw.edu

[†]Current address: Schulich School of Medicine & Dentistry, Western University London, ON, Canada N6A 5C1

Hormones can transmit signals through adenosine 3',5'-monophosphate (cAMP) to precise intracellular locations. The fidelity of these responses relies on the activation of localized protein kinase A (PKA) holoenzymes. Association of PKA regulatory (RII) subunits with A-kinase anchoring proteins (AKAPs) confers location, and catalytic (C) subunits phosphorylate substrates. Single-particle electron microscopy demonstrated that AKAP79 constrains RII-C sub-assemblies within 150 to 250Å of its targets. Native mass spectrometry established that these macromolecular assemblies incorporated stoichiometric amounts of cAMP. Chemical-biology and live-cell imaging techniques revealed that catalytically active PKA holoenzymes remained intact within the cytoplasm. In contrast, little, if any PKA activity was detected in the nucleus. Hence the parameters of anchored PKA holoenzyme action are much more restricted than originally anticipated.

Summary: PKA catalytic subunit does not dissociate from AKAP-anchored PKA holoenzymes at physiologically relevant cAMP concentrations.

Classical *in vitro* biochemistry and elegant structural studies have led to a commonly held view that active PKA catalytic subunit dissociates from the regulatory subunit dimer in the presence of excess cAMP (*1-4*). Yet the utility of this rudimentary mechanism inside cells remains unclear (*5*). Single-particle negative-stain electron microscopy (EM) analysis of AKAP79:PKA holoenzyme complexes (AKAP79:2RII:2C) detected a range of conformationally distinct species (Fig. 1, A through D and fig. S1). A set of ~14,000 particles was subjected to reference-free 2D classification using RELION (*6*). Poorly-aligned classes were discarded over multiple iterations

to reveal an ensemble of three-lobed assemblies in which the peripheral densities are observed at different distances from each other. These range from 150Å in the compact configuration to 250Å in the extended conformation (Fig. 1E). The tandem peripheral lobes represent the catalytic subunit in complex with the cAMP binding domains of RII (*7*), whereas the central density represents the A-kinase anchoring protein-RII dimer interface (Fig. 1E). Thus AKAP79 constrains each sub-assembly of regulatory and catalytic subunits to within 250Å of substrates. We surmise that the restricted movement of the anchored C subunit in this configuration augments phosphorylation of local substrates that are either interacting with the AKAP (Fig. 1F) or in proximity to the peripheral lobes of the extended PKA holoenzyme (Fig. 1G).

An implication of our structural model is that although local cAMP production stimulates kinase activity, AKAP79:2RII:2C assemblies can remain intact. Native mass spectrometry (MS) allows the measurement of molecular mass and is used to determine the stoichiometry of intact protein complexes in the gas phase (*8-10*). In the presence of cAMP, which co-purifies with RII, we observed higher order complexes, including the intact 2RII:2C PKA holoenzyme and the pentameric AKAP79:2RII:2C assembly (Fig. 1H, fig. S1 and tables S1-2). These experiments infer a minimal disruption of the AKAP-PKA architecture even in the presence of cAMP.

To address the relative stability of the pentameric AKAP79:2RII:2C assembly in the presence of elevated cAMP we performed pulldown experiments with a fragment of the anchoring protein $AKAP79^{297-427}$. Retention of anchored C subunits in the presence of increasing concentrations of cAMP was assessed by quantification of Coomassie blue stained protein (Fig.1I and inset). At physiological concentrations of cAMP (1 to 2 μM) most of the C subunit (~70 to 80%) remained associated with the $AKAP79^{297-427}$-RII complex (Fig.1I and inset). Substantial release of the C subunit was only evident at supraphysiological levels of cAMP (Fig. 1I; 10 to 90 μM) and no change in binding of RII to $AKAP79^{297-427}$ was observed. In control experiments, 5'-AMP (100μM), a degradation product of cAMP, did not alter anchored holoenzyme composition (Fig. 1I). Thus physiological amounts of cAMP promote minimal release of the C subunit from the anchored holoenzyme *in vitro*.

Additional studies used high resolution native MS to evaluate cAMP occupancy in PKA holoenzyme complexes. At basal cAMP concentrations, multiple charge states of 2RII:C sub-complexes were observed between m/z 5700 to 6300. These species preferentially contained 2, but up to 4, molecules of cAMP (fig. S1). When analysis was done at higher concentrations of cAMP (5 μM), the predominant species exhibited cyclic nucleotide occupancy of 4 moles per RII dimer (fig. S1 and table S3). Of note, the C subunit remained attached under these conditions (fig. S1). Thus, we can conclude that a substantial proportion of the PKA catalytic subunit remained associated with the $AKAP79^{297-427}$-RII dimer when cAMP-binding sites were occupied.

For a more stringent *in situ* test, we monitored the integrity of cellular AKAP-PKA complexes in response to ligand activation. AKAP79 or AKAP18γ complexes were immunoprecipitated from cell lysates prepared after stimulation of cells with the β-adrenergic agonist isoproterenol (Iso; 1μM). Immunoblot analysis detected equivalent amounts of C subunit in samples from cells stimulated with isoproterenol or vehicle control (Fig. 2, A and B; top panels, lane 2). Local cAMP flux is controlled through a balance of second messenger production by adenylyl cyclases

and degradation by phosphodiesterases (PDEs) (*11, 12*). Cells were stimulated with isoproterenol in the presence of the general PDE inhibitor 3-isobutyl-1-methylxanthine (IBMX), the selective PDE3 inhibitor milrinone, or the PDE4-specific inhibitor rolipram (*13*, *14*). The composition of AKAP79-PKA complexes was assessed by immunoblot. Intact complexes were detected in control and Iso treated samples (Fig. 2C, lanes 1 and 2). Inclusion of rolipram promoted full dissociation of the C subunit (Fig. 2C, lane 3). Likewise, application of IBMX induced release of the C subunit from AKAP complexes (Fig. 2C, lane 5). In contrast, inclusion of milrinone had little effect, indicating that PDE3 is non-functional in these AKAP79-PKA microdomains (Fig. 2C, lane 4). Kinase activation was monitored by immunoblot detection of phospho-PKA substrates (Fig. 2C, bottom panel). Similar findings were obtained upon analysis of AKAP18γ complexes, and when prostaglandin E1 (PGE_1) or epinephrine were used as agonists (fig. S2). Treatment with rolipram alone did not activate PKA or release C subunits (Fig. 2C, lane 6). Thus, native production of cAMP in response to physiological effectors of GPCR signaling appears not to promote C subunit release from anchored PKA holoenzymes.

Förster Resonance Energy Transfer (FRET) was used to investigate PKA holoenzyme composition in real time (*15, 16*). Initially, we used RII conjugated to cyan fluorescent protein (RII-CFP) and C-subunit conjugated to yellow fluorescent protein (C-YFP) as intermolecular FRET probes to monitor the integrity of the PKA holoenzyme after agonist stimulation of cells (Fig. 2D). Isoproterenol promoted minimal change in the CFP/YFP FRET ratio over time courses of 400 sec (Fig. 2, E and H, black), consistent with negligible dissociation of the PKA holoenzyme. In contrast, pre-incubation of cells with rolipram before stimulation with β-adrenergic agonist triggered a pronounced and time-dependent reduction in the FRET ratio (Fig. 2, F and H; red). Thus, dissociation of the PKA holoenzyme only occurred if cAMP accumulated to supraphysiological concentrations. Pretreatment of cells with the PDE3 inhibitor milrinone had little effect on the FRET response (Fig. 2, G and H, grey). Comparable FRET recordings were obtained when PGE_1 was used as the agonist (fig. S2).

The ICUE3 FRET biosensor detects agonist-responsive accumulation of cAMP (Fig. 2I) (*17*). Stimulation of cells with isoproterenol or PGE_1 promoted transient increases in the FRET signal (Fig. 2J, black and fig. S2). This response was enhanced by addition of rolipram (Fig. 2J, red and fig. S2). However, the highest amounts of cAMP production (15 fold above physiological levels) were recorded upon application of forskolin, a direct activator of adenylyl cyclases and common tool in cAMP research (Fig. 2J, blue). Thus, forskolin sustains supraphysiological accumulation of cAMP to concentrations far above those induced by β-agonists.

We investigated the effect of recurrent stimulation of cAMP synthesis on PKA holoenzyme integrity with the same biosensors. After an initial pulse of isoproterenol, the drug was washed out for 500 seconds before application of a second stimulus (Fig. 2, K and L). Intermolecular FRET revealed that RII-CFP and C-YFP remained in proximity over the duration of these experiments (Fig. 2K, black). As expected, co-stimulation of cells with isoproterenol and rolipram initiated cycles of holoenzyme dissociation and reformation (Fig. 2K, red). Complementary biochemical experiments revealed that washout of rolipram and isoproterenol promoted reformation of AKAP79-PKA holoenzyme over a similar time course (fig. S2). Using the ICUE3 biosensor, we demonstrated that isoproterenol induces a transient rise in the cellular concentration of cAMP that approaches baseline during washout (Fig. 2L, black). A second

application of agonist then initiates another round of cAMP production. In contrast, co-stimulation with rolipram produces two additive phases of intracellular cAMP accumulation (Fig. 2L, red). Collectively these experiments demonstrate that PDE4 modulates cAMP microdomains surrounding anchored and intact PKA holoenzymes

Proximity ligation assays (PLA) detect endogenous protein-protein interactions that occur within 40 to 60 nm (*18*). Unstimulated and agonist-treated HEK293 cells were fixed, stained with antibodies to RII and C subunits and subjected to the PLA amplification protocol prior to imaging of PLA puncta (fig. S2). Image intensity profiling of PLA puncta showed the distribution of intact PKA holoenzymes (Fig. 2, M through O). The number of the puncta per cell indicated the extent of RII-C interactions under each experimental condition (Fig. 2P). Treatment with isoproterenol did not appreciably change the PLA signal as compared to unstimulated control cells (Fig. 2, M, N and P). In contrast, treatment of cells with isoproterenol and rolipram reduced the number and intensity of PLA puncta (Fig. 2, O and P). Immunoblot detection of endogenous RII and C in HEK293 cell lysates confirmed the same trend (fig. S2). Thus physiological agonists that mobilize cAMP signaling promote very little dissociation of native PKA holoenzymes inside cells.

To test whether covalent coupling of RII to the C subunit would alter PKA action inside cells, we generated a construct that encodes RIIα and Cα in one polypeptide, creating a non-dissociable PKA fusion enzyme designated "R2C2" (Fig. 3A). To exploit this tool in a simplified genetic background, we used CRISPR-Cas9 editing to disrupt the *PRKAR2A*, *PRKAR2B* and *PRKACA* genes in U2OS human osteosarcoma cells (triple KO U2OS$^{R2A/R2B/CA}$). Loss of protein expression due to gene-editing was confirmed by immunoblot (Fig. 3B, lane 2, upper three panels). Rescue upon expression of R2C2 was confirmed by immunoblot (Fig. 3C, lane 3; top panel). Activity profiling using the phospho-PKA substrates antibody confirmed that isoproterenol responsive PKA activation was reduced to baseline levels in triple KO U2OS$^{R2A/R2B/CA}$ cells (fig. S3). Further removal of the *PRKACB* gene was unsuccessful, suggesting that ablation of both *PRKAC* genes could be a lethal event. Yet, quadruple KO U2OS$^{R2A/R2B/CA/CB}$ cells survived if gene editing was performed in cells stably expressing murine R2C2 (fig. S3).

We next used AKAR4 biosensors that measure PKA activity via changes in FRET to assess how compartmentalization affects free and fused PKA activity (Fig. 3D) (*19*). Rapid increases in cytoplasmic FRET responses were recorded in U2OS$^{R2A/R2B/CA}$ cells rescued with murine RIIα and Cα (Fig. 3, E and F, orange). Importantly, cells expressing the R2C2 fusion protein generated isoproterenol responses of similar magnitude and duration (Fig. 3, E and F, green). There was no detectable FRET response to agonist stimulation in the U2OS$^{R2A/R2B/CA}$ deletion background or in cells expressing a catalytically inactive mutant of the RII-C fusion (R2C2^{K72A}; Fig. 3, E and F, grey and fig. S3). Thus, covalent coupling of the PKA subunits does not impair cAMP signaling in the cytoplasm and can reconstitute endogenous kinase activity.

To further underscore this latter point, we used rapamycin-regulated heterodimerization to "*pharmacologically lock"* FRB-domain tagged C-subunits (FRB-C) to FK506-binding protein domain tagged RII dimers (FKBP-RII) in the context of the AKAP18 complex. In this system, the small molecule rapamycin bridges the tagged proteins to maintain a stable complex (Fig.

3G). Immunoblot analyses of AKAP18 immune complexes from cells expressing FKBP-RII and FRB-C revealed that both proteins were associated after stimulation of cells with isoproterenol in the absence of rapamycin (Fig. 3H, top panel, lane 2). As before, administration of isoproterenol and rolipram together caused supraphysiological accumulation of cAMP and abolished this interaction (Fig. 3H, top panel, lane 3). Conversely, application of rapamycin locks the FRB-C/FKBP-RII sub-complex together, even when cells are treated with isoproterenol plus rolipram (Fig. 3H, top panel, lane 6).

Cell-based studies in triple knockout U2OS cells confirmed that cytoplasmic FRET responses to isoproterenol were robust (Fig. 3I, orange), even after pharmacological locking of this modified PKA holoenzyme with rapamycin (Fig. 3I, blue). Isoproterenol treatment of cells in the presence of rolipram has no additional effect (fig. S3). Thus cytoplasmic PKA signaling is sustained when the C subunit and the RII dimer are chemically constrained.

We monitored nuclear PKA activity with an AKAR biosensor targeted to the nucleus via a nuclear localization signal (AKAR4^{NLS}) (*19*). FRET signals were negligible in both wildtype and U2OS$^{R2A/R2B/CA}$ cells stimulated with isoproterenol (fig. S3, Fig. 3J and 3K, grey). In fact, detection of any nuclear FRET required supraphysiological accumulation of cAMP upon stimulation of adenylyl cyclases with 20μM forskolin in the presence of IBMX for 30 minutes. Under these extreme conditions, rescue with murine RIIα and Cα resulted in a gradual increase in FRET over 15 minutes (Fig. 3, J and K, orange). In contrast, cells expressing R2C2 showed greatly diminished nuclear FRET responses (Fig. 3, J and K, green). Chemically locking FRB-C subunits to FKBP-RII dimers with rapamycin also impairs the nuclear AKAR4 FRET responses in cells treated with isoproterenol and rolipram (fig. S3). Together, these results demonstrate that cytoplasmic activation of PKA is a rapid event, whereas nuclear signaling requires persistent and supraphysiological accumulation of cAMP.

This latter finding has ramifications for nuclear cAMP-responsive events. The cAMP response element binding protein CREB is a transcription factor that is a substrate for several kinases including Akt, MSK1/2 and PKA (*20-22*). We used immunofluorescence detection of nuclear pSer133 to monitor CREB phosphorylation *in situ* (*23*). Little, if any phosphorylation of CREB was evident after stimulation of U2OS$^{R2A/R2B/CA}$ cells with isoproterenol for 30 minutes (Fig. 3, L through O). Expression of R2C2 led to a small increase in the Iso-stimulated nuclear pSer133 signal (Fig. 3, P through S), whereas overexpression of murine RIIα and Cα strongly augmented this response (Fig. 3, T through W). Amalgamated fluorescence intensities of the pSer133 signal (35-55 cells, each condition) are presented in Fig. 3X. These findings tally with the FRET data (Fig. 3K and S3) showing that the R2C2 fusion has limited access to the nucleus. Hence, PKA phosphorylation of CREB and subsequent nuclear transcriptional events may be limited to instances of long-term or supraphysiological accumulation of cAMP. This is in stark contrast to hormonal responses that evoke rapid physiological pulses of cAMP to drive anchored PKA activation.

We generated an analog-sensitive form of R2C2 that is exclusively modulated by the cell-permeable kinase inhibitor 1-napthylmethyl-PP1 (1-NM-PP1; Fig. 4A) (*24, 25*). Engineering this pharmacologically tractable and fused form of PKA was achieved by substituting the gatekeeper methionine in the catalytic moiety of R2C2 with alanine (M120A). *In situ*

characterization of this synthetic analog-sensitive kinase in U2OS$^{R2A/R2B/CA}$ cells was achieved using an AKAP-derived PKA activity reporter (AKAP18^{RBS}-AKAR4; Fig. 4B). In cells expressing wildtype R2C2, isoproterenol (1μM) stimulation induced a FRET response within 10 sec that was refractory to 1-NM-PP1 (Fig. 4C, green). The rate and magnitude of the FRET response was attenuated in cells expressing R2C2 M120A, a common property of analog-sensitive kinases (*25*). However, application of 1-NM-PP1 (2μM) to these cells reduced the FRET signal to baseline, indicating strong inhibition of the analog-sensitive kinase (Fig. 4C, blue). Thus 1-NM-PP1 is an efficient inhibitor of R2C2 M120A in situ.

We used this chemically controllable form of fused PKA to examine phosphorylation of local extra-nuclear substrates. The mitochondrial anchoring protein D-AKAP-1 sequesters PKA at mitochondria to regulate phosphorylation of the pro-apoptotic protein BAD (Fig. 4D) (*26*). PKA phosphorylation of BAD Ser155 blocks apoptosis through a mechanism involving recruitment of 14-3-3 proteins to suppress programmed cell death (Fig. 4D) (*27-29*). BAD phosphorylation on serine 155 was robustly stimulated by isoproterenol in WT U2OS cells and this effect was blunted in triple knockout cells (fig. S4). Confocal imaging confirmed that D-AKAP-1 and BAD are detected at mitochondria (fig. S4), whereas proximity ligation assays detected puncta that are indicative of an interaction between these two proteins (fig. S4). In triple knockout cells expressing the R2C2 WT and R2C2 M120A mutants, immunoblot analysis confirmed that these modified kinases effectively phosphorylated BAD Ser155 after treatment of cells with isoproterenol (Fig. 4E; top panel, lanes 1-4). Control immunoblots monitored the expression of the PKA fusion enzymes and GAPDH served as loading controls (Fig. 4E; mid and bottom panels). Application of 1-NM-PP1 (2μM) inhibited the activity of R2C2 M120A and blocked phosphorylation of BAD Ser155 (Fig. 4E; top panel; lane 6). Normalized BAD pSer155 data from three independent experiments is presented in Fig. 4F. With this tool, we could test whether local activation of PKA is inhibitory toward apoptosis.

We induced apoptosis in triple knockout cells expressing R2C2 M120A by treatment with the chemotoxic agent etoposide (Fig. 4, G and H) (*30*). Cell death was assessed as accumulation of a fluorescent product of caspase 3 or 7-mediated proteolysis (green, Fig. 4G) and nuclear condensation observed upon staining DNA with 4',6-diamidino-2-phenylindole (DAPI, magenta, Fig. 4G). Unstimulated cells exhibit low levels of apoptosis (Fig. 4G, left panel and Fig. 4H). Etoposide treatment promotes cell death (Fig. 4G, left-mid panel and Fig. 4H). Stimulation of R2C2 activity with β-AR agonists (Iso and formoterol) was protective as it substantially reduced the apoptotic index (Fig. 4G, mid-right panel and Fig. 4H). Application of 1-NM-PP1 blocked this protective effect (Fig. 4G, right panel and Fig. 4H, blue). Thus, fused RII and C subunits can substitute for endogenous PKA in the modulation of local cellular events.

Contrary to current dogma, our results show that anchored PKA holoenzymes remain intact or in immediate proximity to anchoring sites and substrates in the presence of cAMP, and that fusion of the kinase moiety to RII supports cAMP signaling in diverse cellular contexts. One exception seems to be PKA action in the nucleus. Within this subcellular compartment we detected minimal PKA activation, even after sustained accumulation of cAMP to supraphysiological levels. Thus phosphorylation of the transcription factor CREB on serine 133 may not proceed directly through PKA. Three factors can account for this view: 1) the well-documented nuclear exclusion of all R subunit isoforms guarantees formation of the PKA holoenzyme solely in the

cytoplasm (*31-35*); 2) cytoplasmic retention of intact but active PKA holoenzymes reduces the availability of free C subunit to enter the nucleus and 3) the heat-stable inhibitor (PKI) affords a failsafe mechanism to rapidly inhibit and export any free C subunit that strays into the nucleus (*36-38*). Consequently, crosstalk with CREB kinases such as calcium-calmodulin dependent protein kinase II (CaMKII), mitogen- and stress-activated protein kinase-1 (MSK1), Akt or ribosomal S6 kinase (RSK) isoforms is more likely to manage cAMP responsive transcription (*22, 39, 40*).

Finally, because AKAP79 constrains intact and catalytically active PKA within 150 to 250Å, we propose that the range of anchored PKA action is much more restricted than originally anticipated (Fig. 1, F and G) (*41*). Another prerequisite for this new model is that the location of these active zones must coincide with microdomains where cAMP concentrations increase and when substrates are available (*11, 42*). This intricate molecular architecture helps explain how common signaling components are assembled to elicit distinct, rapid and transient endocrine responses.

REFERENCES

1. D. A. Walsh, J. P. Perkins, E. G. Krebs, An adenosine 3',5'-monophosphate-dependent protein kinase from rabbit skeletal muscle. *J. Biol. Chem.* 243, 3763-3765 (1968).

2. R. L. Potter, S. S. Taylor, Relationships between structural domains and function in the regulatory subunit of cAMP-dependent protein kinases I and II from porcine skeletal muscle. *J. Biol. Chem.* 254, 2413-2418 (1979).

3. D. R. Knighton *et al.*, Crystal structure of the catalytic subunit of cyclic adenosine monophosphate-dependent protein kinase. *Science* 253, 407-414 (1992).

4. P. Zhang *et al.*, Structure and allostery of the PKA RIIbeta tetrameric holoenzyme. *Science* 335, 712-716 (2012).

5. L. K. Langeberg, J. D. Scott, Signalling scaffolds and local organization of cellular behaviour. *Nat Rev Mol Cell Biol* 16, 232-244 (2015).

6. S. H. Scheres, RELION: implementation of a Bayesian approach to cryo-EM structure determination. *J Struct Biol* 180, 519-530 (2012).

7. F. D. Smith *et al.*, Intrinsic disorder within an AKAP-protein kinase A complex guides local substrate phosphorylation. *eLife* 2, e01319 (2013).

8. A. J. Heck, Native mass spectrometry: a bridge between interactomics and structural biology. *Nature methods* 5, 927-933 (2008).

9. M. G. Gold *et al.*, Architecture and dynamics of an A-kinase anchoring protein 79 (AKAP79) signaling complex. *Proc Natl Acad Sci U S A* 108, 6426-6431 (2011).

10. D. P. Byrne *et al.*, cAMP-dependent protein kinase (PKA) complexes probed by complementary Differential Scanning Fluorimetry and Ion Mobility-Mass Spectrometry. *Biochem J* 473, 3159-3175 (2016).

11. M. Zaccolo, T. Pozzan, Discrete microdomains with high concentration of cAMP in stimulated rat neonatal cardiac myocytes. *Science* 295, 1711-1715. (2002).

12. C. W. Dessauer, Adenylyl cyclase--A-kinase anchoring protein complexes: the next dimension in cAMP signaling. *Mol. Pharmacol.* 76, 935-941 (2009).

13. P. J. Silver, Biochemical aspects of inhibition of cardiovascular low (Km) cyclic adenosine monophosphate phosphodiesterase. *Am J Cardiol* 63, 2A-8A (1989).

14. S. L. Jin, T. Bushnik, L. Lan, M. Conti, Subcellular localization of rolipram-sensitive, cAMP-specific phosphodiesterases. Differential targeting and activation of the splicing variants derived from the PDE4D gene. *J Biol Chem* 273, 19672-19678 (1998).

15. J. Zhang, R. E. Campbell, A. Y. Ting, R. Y. Tsien, Creating new fluorescent probes for cell biology. *Nat Rev Mol Cell Biol* 3, 906-918 (2002).

16. J. D. Scott, A. C. Newton, Shedding light on local kinase activation. *BMC biology* 10, 61 (2012).

17. L. M. DiPilato, J. Zhang, The role of membrane microdomains in shaping beta2-adrenergic receptor-mediated cAMP dynamics. *Mol Biosyst* 5, 832-837 (2009).

18. O. Soderberg *et al.*, Proximity ligation: a specific and versatile tool for the proteomic era. *Genet Eng (N Y)* 28, 85-93 (2007).

19. K. J. Herbst, M. D. Allen, J. Zhang, Spatiotemporally regulated protein kinase A activity is a critical regulator of growth factor-stimulated extracellular signal-regulated kinase signaling in PC12 cells. *Mol Cell Biol* 31, 4063-4075 (2011).

20. K. T. Raibowol *et al.*, The catalytic subunit of cAMP-dependent protein kinase induces expression of genes containing cAMP-responsive enhancer elements. *Nature* 336, 83-86 (1988).

21. M. Johannessen, U. Moens, Multisite phosphorylation of the cAMP response element-binding protein (CREB) by a diversity of protein kinases. *Front Biosci* 12, 1814-1832 (2007).

22. M. Deak, A. D. Clifton, L. M. Lucocq, D. R. Alessi, Mitogen- and stress-activated protein kinase-1 (MSK1) is directly activated by MAPK and SAPK2/p38, and may mediate activation of CREB. *EMBO J* 17, 4426-4441 (1998).

23. J. C. Chrivia *et al.*, Phosphorylated CREB binds specifically to the nuclear protein CBP. *Nature* 365, 855-859 (1993).

24. D. J. Morgan *et al.*, Tissue-specific PKA inhibition using a chemical genetic approach and its application to studies on sperm capacitation. *Proc Natl Acad Sci U S A* 105, 20740-20745 (2008).

25. M. S. Lopez, J. I. Kliegman, K. M. Shokat, The logic and design of analog-sensitive kinases and their small molecule inhibitors. *Methods Enzymol* 548, 189-213 (2014).

26. H. Harada *et al.*, Phosphorylation and inactivation of BAD by mitochondria-anchored protein kinase A. *Mol. Cell* 3, 413-422 (1999).

27. J. M. Lizcano, N. Morrice, P. Cohen, Regulation of BAD by cAMP-dependent protein kinase is mediated via phosphorylation of a novel site, Ser155. *Biochem J* 349, 547-557 (2000).

28. Y. Tan, M. R. Demeter, H. Ruan, M. J. Comb, BAD Ser-155 phosphorylation regulates BAD/Bcl-XL interaction and cell survival. *J Biol Chem* 275, 25865-25869 (2000).

29. K. Virdee, P. A. Parone, A. M. Tolkovsky, Phosphorylation of the pro-apoptotic protein BAD on serine 155, a novel site, contributes to cell survival. *Curr Biol* 10, R883 (2000).

30. E. H. Cheng, T. V. Sheiko, J. K. Fisher, W. J. Craigen, S. J. Korsmeyer, VDAC2 inhibits BAK activation and mitochondrial apoptosis. *Science* 301, 513-517 (2003).

31. L. B. Lester, V. M. Coghlan, B. Nauert, J. D. Scott, Cloning and characterization of a novel A-kinase anchoring protein: AKAP220, association with testicular peroxisomes. *J. Biol. Chem.* 272, 9460-9465 (1996).

32. C. K. Means *et al.*, An entirely specific type I A-kinase anchoring protein that can sequester two molecules of protein kinase A at mitochondria. *Proceedings of the National Academy of Sciences of the United States of America* 108, E1227-1235 (2011).

33. H. Abrahamsen, T. Vang, K. Tasken, Protein kinase A intersects SRC signaling in membrane microdomains. *J Biol Chem* 278, 17170-17177 (2003).

34. B. S. Skalhegg *et al.*, Location of cAMP-dependent protein kinase type I with the TCR-CD3 complex. *Science* 263, 84-87 (1994).

35. P. Zhang *et al.*, An Isoform-Specific Myristylation Switch Targets Type II PKA Holoenzymes to Membranes. *Structure* 23, 1563-1572 (2015).

36. J. D. Scott, E. H. Fischer, K. Takio, J. B. DeMaille, E. G. Krebs, Amino acid sequence of the heat-stable inhibitor of the cAMP-dependent protein kinase from rabbit skeletal muscle. *Proc. Natl. Acad. Sci. U.S.A.* 82, 5732-5736 (1985).

37. W. Wen *et al.*, Heat-stable inhibitors of cAMP-dependent protein kinase carry a nuclear export signal. *J. Biol. Chem.* 269, 32214-32220 (1994).

38. W. Wen, J. L. Meinkoth, R. Y. Tsien, S. S. Taylor, Identification of a signal for rapid export of proteins from the nucleus. *Cell* 82, 463-473 (1995).

39. H. Bito, K. Deisseroth, R. W. Tsien, CREB phosphorylation and dephosphorylation: a Ca(2+)- and stimulus duration-dependent switch for hippocampal gene expression. *Cell* 87, 1203-1214 (1996).

40. G. Y. Wu, K. Deisseroth, R. W. Tsien, Activity-dependent CREB phosphorylation: convergence of a fast, sensitive calmodulin kinase pathway and a slow, less sensitive mitogen-activated protein kinase pathway. *Proc Natl Acad Sci U S A* 98, 2808-2813 (2001).

41. E. M. Snyder *et al.*, Role for A kinase-anchoring proteins (AKAPS) in glutamate receptor trafficking and long term synaptic depression. *J Biol Chem* 280, 16962-16968 (2005).

42. B. Lygren *et al.*, AKAP complex regulates Ca2+ re-uptake into heart sarcoplasmic reticulum. *EMBO Rep* 8, 1061-1067 (2007).

43. B. Kastner *et al*., GraFix: sample preparation for single-particle electron cryomicroscopy. *Nature Methods* 5, 53-55 (2008).

44. C. Suloway *et al*., Automated molecular microscopy: the new Leginon system. *J. Struct Biol*. **151**, 41-60 (2005).

45. N. R. Voss *et al*., DoG Picker and TiltPicker: software tools to facilitate particle selection in single particle electron microscopy. *J Struct Biol.* 166, 205-213 (2009).

46. M. T. Marty *et al*., Bayesian deconvolution of mass and ion mobility spectra: from binary interactions to polydisperse ensembles. *Analytical Chemistry* 87, 4370-4376 (2015).

47. O. Soderberg *et al.*, Characterizing proteins and their interactions in cells and tissues using the in situ proximity ligation assay. *Methods* 45, 227-232 (2008).

Acknowledgements

We would like to thank Katherine Forbush for technical support, K.F. and Natalie Pollett for molecular biology and cell culture assistance, all the members of the Scott Lab for critical discussions, Tony Cooke for technical assistance with FRET microscopy, and finally, Melanie Milnes for administrative support. This work was supported by the following grants from the National Institutes of Health: 5R01DK105542 (J.D.S.), 4P01DK05441 (J.D.S.), 1R01GM120553 (D.V.), and BBSRC grant BB/L009501/1 (C.E.), North West Cancer Research grant CR1037 (P.E.) and Core funding from the IIB, FHLS, University of Liverpool (C.E. and P.E.).

F.D.S. and J.D.S. conceived of and supervised the project. F.D.S., J.L.E., P.J.N, D.B., M.V., C.E., P.E. and J.D.S. designed the experiments. F.D.S., J.L.E., P.J.N, D.B., M.V., C.E., and P.E.

performed experiments. F.D.S., J.L.E., P.J.N, D.B., M.V., C.E., P.E. and J.D.S. analyzed the data. D.V. provided guidance and software for EM experiments. I.S. provided guidance and support for MS experiments with Thermo EMR. L.K.L designed and prepared figures. F.D.S, L.K.L. and J.D.S. wrote the manuscript.

Fig.1. AKAP-PKA holoenzyme assemblies remain intact upon cAMP stimulation. **(A)** SDS-PAGE and stain-free visualization of a purified complex of AKAP79, RII and C subunits of PKA. **(B)** Stain-free visualization on native gels of intact AKAP79-PKA holoenzyme complex. **(C-E)** Representative negative-stain EM micrographs of AKAP79:2RII:2C single particles. **(D)** Traces outlining the selected particles in (C). **(E)** Reference-free class averages from RELION 2D alignment and classification showing range of particle lengths. **(F-G)** Schematics illustrating the flexibility and range of motion in AKAP79-anchored PKA holoenzymes. A compact state may favor the phosphorylation of associated substrates (F), while an extended conformation may allow PKA to act on multiple distinct local substrates (G). **(H)** Zero charge state native nESI mass spectrum of RII+C+AKAP$^{297-427}$ complexes. The stoichiometry of AKAP79$^{297-427}$ (grey), RII (green), C subunit (orange), and cAMP (yellow) is indicated. **(I)** Percentage of C subunit bound to AKAP79$^{297-427}$–PKA complexes after incubation with increasing cAMP concentrations. Data are presented as means ± SEM. Inset shows Coomassie blue staining of proteins in pull-down experiments.

Fig. 2. Anchored PKA holoenzyme dynamics upon ligand stimulation. Western blot analysis of PKA C and RII subunits in **(A**) AKAP79 or **(B)** AKAP18γ immunoprecipitates (IP) after isoproterenol stimulation (Iso). **(C)** IP and Western blot analysis of AKAP79 complexes isolated in the presence of phosphodiesterase inhibitors. **(D)** Schematic depicting RII-CFP and C-YFP intermolecular FRET. **(E-H)** FRET analysis of holoenzyme dissociation in HEK293 cells. **(E)** Time course of representative cells (0-400sec) stimulated with isoproterenol. (F) Iso + PDE4 inhibitor rolipram. **(G)** Iso + PDE3 inhibitor milrinone. **(H)** Amalgamated data from 25 recordings under each experimental condition. **(I)** Schematic depicting ICUE3 cAMP FRET sensor. **(J)** ICUE3 FRET recordings show cAMP production in response to Iso (black), Iso + rolipram (red), and forskolin (blue). The number of experiments is indicated. **(K-L)** FRET analysis upon two trains of hormonal stimulation. **(K)** Intermolecular FRET analysis of holoenzyme dissociation in HEK293 cells upon two trains of stimulation with isoproterenol (black) and Iso + PDE4 inhibitor rolipram (red). **(L)** Monitoring cAMP accumulation with ICUE3 FRET sensor in response to isoproterenol (black) and Iso + PDE4 inhibitor rolipram (red). Amalgamated data from 25 recordings under each experimental condition. **(M-O)** Proximity ligation (PLA) signal intensity projections show RII-C interactions in **(M)** Unstimulated, **(N)** Iso-stimulated, and **(O)** Iso + rolipram treated HEK293 cells. **(P)** Quantification of PLA puncta/cell using Fiji/ImageJ. All data are presented as means ± SEM.

Fig. 3. CRISPR-Cas9 PKA triple knockout and rescue with an RII-C fusion. **(A)** Schematic depicting the R2C2 PKA fusion enzyme. **(B)** Immunoblots confirming knockout of PKA subunit proteins: (top) RIIα, (upper-mid) RIIβ, (lower-mid) C-subunit. Ponceau (bottom) staining shows equal loading in U2OS$^{R2A/R2B/CA}$ cells. **(C)** Western blotting for PKA C subunit to confirm expression of R2C2 fusion. **(D)** Schematic of AKAR4 PKA activity biosensor. **(E)** Representative cells showing cytoplasmic AKAR4 FRET response upon rescue with (left) RIIα and Cα and (right) R2C2 fusion. **(F)** Cytoplasmic FRET recordings in triple knockout U2OS$^{R2A/R2B/CA}$ cells (grey) and cells rescued with R2C2 fusion (green) or WT RIIα and Cα (orange). **(G)** Schematic of rapamycin induced heterodimerization of PKA subunits. **(H)** Immunoblots showing that rapamycin chemically locks the PKA holoenzyme at supraphysiological concentrations of cAMP. **(I)** Cytoplasmic FRET recordings in response to Iso (1 μM) stimulation in U2OS$^{R2A/R2B/CA}$ cells expressing FKBP-RII and FRB-C in the presence (blue) or absence (orange) of rapamycin (100 nM). **(J)** Montage of cells showing nuclear AKAR4 FRET signals upon rescue with (left) RIIα and Cα, or (right) R2C2 fusion. **(K)** Nuclear FRET recordings in U2OS$^{R2A/R2B/CA}$ cells (grey) and cells rescued with R2C2 fusion (green) or wild-type RIIα and Cα (orange). **(L-W)** immunofluorescence detection of phospho-CREB Ser133 (yellow; panels L, N, P, R, T and V) in U2OS$^{R2A/R2B/CA}$ cells rescued with R2C2 (P, Q, R and S) or expression of murine PKA subunits (T & U and V & W). Composite images (panels M, O, Q, S, U and W) reveal staining for RIIα (blue) and actin (grey). **(X)** Quantification of CREB pSer133 immunofluorescence. All data are presented as means ± SEM.

Fig. 4. Chemical-genetic and pharmacological control of mitochondrial PKA action. **(A)** Schematic depicting the introduction of an analog-sensitive kinase mutation into the R2C2 PKA fusion enzyme. The activity of this pharmacologically-controlled fusion kinase was monitored in U2OS$^{R2A/R2B/CA}$ cells. **(B)** Representative cells showing cytoplasmic AKAR FRET signals at selected time points from cells expressing (top) R2C2 and (bottom) the 1-NM-PP1 sensitive R2C2 M120A mutant. The left image in both panels shows expression of the FRET reporter. The other panels show pseudo-color images of the FRET intensity at one time point prior to stimulation (-45 sec), one time point after stimulation with isoproterenol (105 sec) and a third time point after addition of 1-NM-PP1 (415 sec). **(C)** Time courses of cytoplasmic AKAR4 FRET responses to Iso (1 μM, time zero) and 1-NM-PP1 (2 μM, 300 sec) in PKA triple knockout cells expressing the (green) R2C2 fusion or (blue) the R2C2 M120A mutant. **(D)** Schematic depicting protective effects of anchored PKA due to phosphorylation of BAD, and resultant release of the pro-survival BCL-2 protein. **(E)** Inhibition of PKA directed BAD pSer155 phosphorylation by 1-NM-PP1 in cells expressing R2C2 M120A. Immunoblot detecting (top) BAD pSer155, (mid) R2C2 and (bottom) GAPDH loading controls. **(F)** Quantification of BAD pSer155 signal from immunoblots from three independent experiments. Data are presented as means ± SEM. **(G)** Fluorescent detection of apoptotic events upon treatment of cells with the apoptotic agent etoposide, plus and minus β-agonists and 1-NM-PP1. Apoptotic cells were detected by (green) activation of caspase and (magenta) condensation of DNA. **(H)** Quantification of percent apoptotic cells from (G). The numbers of cells monitored are indicated above each column. Data are presented as means ± SEM.

Supplementary Materials for

Local protein kinase A action proceeds through intact holoenzymes

F. Donelson Smith[1], Jessica L. Esseltine[1*], Patrick J. Nygren[1], David Veesler[3], Dominic P. Byrne[2], Matthias Vonderach[2], Ilya Strashnov[4], Claire E. Eyers[2], Patrick A. Eyers[2], Lorene K. Langeberg[1] and John D. Scott[1*]

correspondence to: scottjdw@uw.edu or smithdon@uw.edu

This PDF file includes:

Materials and Methods

cDNAs, Cloning and Mutagenesis

The FRET biosensor constructs for AKAR4^{NES}, AKAR4^{NLS} and ICUE3 were kindly provided by Dr. Jin Zhang (UC San Diego). The R2C2 PKA fusion construct was cloned using Gibson Assembly of PCR products into pcDNA3. The construct consists of full length mouse RIIα cDNA, a segment encoding a linker peptide (WDPGSGSLEAGCKNFFPRSFTSCGSLEGGSAAA), the full-length mouse PKA-Cα cDNA and an epitope tag (AAALEHHHHHH*). Mutagenesis to introduce the "kinase-dead" or analog-sensitive mutations (Lys507Ala or Met555Ala in the full-length R2C2 polypeptide) was performed using inverse PCR with Phusion polymerase (NEB), followed by phosphorylation and ligation of free ends. All oligonucleotides and geneBlock fragments were purchased from Integrated DNA Technologies. All other molecular biology procedures followed standard protocols.

Cell Culture

U2OS cells were a gift from Dr. Heidi Hehnly (SUNY Upstate) and were tested by DDC Medical with results verified by ATCC STR profiling. HEK293A (ThermoFisher) cells were cultured in DMEM-H plus 10% FBS and penicillin/streptomycin (ThermoFisher). U2OS cells were cultured in DMEM-H containing 20 mM HEPES pH 7.4, 10% FBS and pen/strep. Cells were passaged 2-3 times per week using TrypLE reagent (ThermoFisher). U2OS$^{R2A/R2B/CA}$ stably expressing R2C2 were created by transfection with the appropriate vectors, selection with G418 (400 μg/ml) for 2-3 weeks, expansion and screening for expression by immunoblot.

CRISPR-Cas9 Editing of PKA Subunit Genes

Vectors encoding sgRNAs and SpCas9-2A-GFP were provided by Horizon Discovery (Cambridge, UK). Multiple sgRNA sequences were tested for each gene targeted. A combination of three individual vectors that worked in initial experiments were co-transfected into U2OS cells using TransIt-LT1 (Mirus). The guide sequences used are as follows:
PRKAR2A guide 5: GTACTTCACCCGCCTGCGCG
PRKAR2B guide 4: ACTCCAGCAGGTCCGCGGGC
PRKACA guide 3: TTTCACTGAAAGGGAGAGAG
Single cells were sorted into 96-well plates by FACS according to GFP fluorescence and individual clones were expanded for testing. Clones were first assayed for loss of protein expression of RIIα, RIIβ and Cα by Western blotting. Clones that had low or undetectable levels of these proteins were further checked for mutations by purification of genomic DNA and PCR of the appropriate region. PCR products were cloned into pCRBluntII (ThermoFisher) and 8-12 individual colonies were chosen for plasmid DNA mini-prep and sequencing.

Negative Stain Electron Microscopy

MBP-AKAP79-6xHis, 6xHis-PKA catalytic (C) subunit, and RIIα–6xHis regulatory subunit were produced in BL21(DE3) pLysS *E. coli* cells (ThermoFisher). Expression was induced with 0.5 mM IPTG for 4 h at 37 ˚C. Proteins were purified using immobilized metal affinity chromatography (IMAC), followed by size-exclusion chromatography (SEC) using a Superdex 200 10/300 GL column (GE Healthcare) with SEC buffer (20 mM HEPES, pH 7.5, 200 mM NaCl). Individual subunits were incubated at 4˚ C overnight with a molar ratio of 1:2.5:3 AKAP79:RII:C in order to promote formation of a complete complex. These assemblies were subjected to SEC again to isolate fully-formed AKAP79:2RII:2C complexes, which were then prepared for EM using the GraFix method (43). Dilute samples were applied to carbon coated grids and negative-stained with uranyl formate. Grids were imaged on a Tecnai T12 TEM at 0.7-1.5 micron defocus ranges using the Leginon package (44). The initial set of ~14,000 particles were autopicked using DoGPicker (45). Particles were refined through multiple rounds to a set of 3513 particles and iteratively sorted by reference-free 2D classification using RELION (6) until high-quality class averages were obtained.

In vitro Pull-down Assays for AKAP79-PKA Complexes

6xHis-PKA catalytic (C) subunit, RIIα-6xHis regulatory subunit and GST-AKAP79 (amino acids 297-427) were produced in BL21(DE3)pLysS *E. coli* cells (Novagen). Expression was induced with 0.5 mM IPTG for 18 h at 18°C. Proteins were purified using either immobilized metal affinity chromatography (IMAC) or glutathione sepharose, followed by size exclusion chromatography using a HiLoad 16/600 Superdex 200 column (GE Healthcare) equilibrated in 50 mM Tris/HCl, pH 7.4, 100 mM NaCl, 10 % (v/v) glycerol and 1 mM DTT. Purified GST-AKAP79$^{297\text{-}417}$ containing a 3C protease cleavage site was incubated on ice for 3 hours with glutathione Sepharose beads, washed five times in binding buffer (50 mM Tris pH 7.4, 0.1M NaCl) and resuspended at a final concentration of ~2μM AKAP79$^{297\text{-}417}$. C-subunit (~16 μM final concentration) and RIIα-subunits (~4 μM final concentration) were incubated with beads in the presence or absence of the indicated concentration of cAMP for 20 mins at 30°C with constant agitation. The supernatant was then removed, and after three washes in binding buffer, complexes were eluted from the beads by incubation with 250 ng of 3C protease for 30 minutes at 30°C. Proteins were analysed by SDS-PAGE on a 12% gel. The percentage of C-subunit bound to the AKAP:RIIa complexes was calculated by densitometry using Image J software, and plotted as a function of cAMP concentration.

Pentamer Formation and Analysis by Ion Mobilization Native Mass Spectrometry

Formation of the pentamer (and associated sub-complexes) was achieved by incubating AKAP79$^{297\text{-}427}$ (0.75 μM), RIIα (1.88 μM) and C-subunit (2.25 μM) (molar ratio 1:2.5:3 with a final volume of 100 μl) in 20 mM HEPES, 100 mM NaCl overnight at 4 °C. No additional cAMP was included. The sample was buffer exchanged into 100 mM NH_4OAc, 1 mM Tris (pH 7.5) prior to native nESI-MS using a Synapt G2-S*i* instrument (Waters). The sprayer voltage was ~1.5 kV, sampling cone was kept at 150 V, source temperature was 80°C, with the instrument operating in mobility mode. Argon pressure in the ion trap and transfer tube was set to $3*10^{-2}$ mbar. The

He cell was 4.5 mbar. Pressure in the ion mobility tube, filled with nitrogen, was 2.8 mbar. Bias voltage for transfer from the ion trap to ion mobility cell was adjusted to 50 V.

Ion Mobilization Native Mass Spectrometry

AKAP binding studies were conducted using a Waters Synapt G2-S*i* instrument. PKA C-subunit (1.5 μM), RIIα (1.5 μM) and AKAP79$^{297\text{-}417}$ (3 μM) were incubated for 20 min at 37°C in 100 mM NH_4OAc and analyzed using borosilicate emitters (Thermo Scientific ES 387). cAMP-dependent experiments were performed on a Thermo Exactive Plus EMR instrument. PKA C-subunit (2.5 μM) and RIIα (2.5 μM) were incubated at room temperature for 10 min in 200 mM NH_4OAc, with cAMP being added to the final stated concentration and incubated again for 10 min prior to nano-Electrospray analysis using borosilicate emitters.

High Resolution Analysis with the Exactive EMR Orbitrap

To determine the stoichiometry of cAMP binding to RII:C complexes, the Exactive EMR Orbitrap (ThermoScientific) was operated at a resolution of 17500 (FWHM at m/z 200). The sprayer voltage was ~1.5 kV. Source ionization was maintained at 200 V.

Data Deconvolution

To assist in MS data interpretation, the native mass spectra were processed using UniDec (46), allowing molecular ions to be assigned and for the generation of the zero charge (deconvoluted) mass spectra.

Cell Lysis, Immunoprecipitation and Immunoblotting

HEK293 or U2OS cells were transiently transfected (TransIT LT1; Mirus) with vectors encoding various proteins according to figures and legends. For most experiments, after 40–48 hr and prior to harvesting, the cells were serum starved in DMEM for 1 hr at 37°C. The cells were then treated with vehicle or drug according to the following conditions. For figure 2, cells were preincubated for 5 min at 37°C with DMSO or PDE inhibitors, followed by addition of 1 μM isoproterenol for a further 5 min at 37°C. Cells were harvested in lysis buffer (25 mM HEPES, pH 7.4, 150 mM NaCl, 1 mM EDTA, 1 mM EGTA, 20 mM NaF, 2% glycerol, 0.3% Triton X-100) containing 100 nM okadaic acid and protease inhibitors. AKAP79 or AKAP18γ complexes were immunoprecipitated with anti-GFP rabbit IgG (Invitrogen) and protein A agarose for 2 hr at 4°C. Beads were washed 4 × 1 ml in lysis buffer. Proteins were separated on 4–12% NuPAGE gradient gels (ThermoFisher) and transferred to nitrocellulose membranes. Primary antibodies used include: PKA catalytic subunit mAb (BD Biosciences clone 5B), 1:1000; RIIα mAb (BD clone 40), 1:2000; GFP mAb (Santa Cruz Biotechnology sc-9996), 1:2000; phospho-PKA substrates rabbit mAb (Cell Signaling Technology (100G7E); 1:1000) were incubated with membranes overnight at 4°C in TBST/Blotto. The membranes were washed extensively in TBST, incubated with HRP-labeled secondary antibodies (Jackson Immunoresearch), washed as before and developed using ECL (ThermoFisher) on an Alpha Innotech MultiImage III with FluoroChem Q software. For re-probing, membranes were stripped with 1X Re-Blot Plus Strong

(Millipore) for 15 minutes and then re-blocked in Blotto before incubation with primary antibodies again.

Proximity Ligation Assays

Cells were cultured on 12-18 mm poly-L-lysine coated glass coverslips. After 24-30 hours, cells were starved for 1 hour and then stimulated with appropriate agonists (see figures). Cells were fixed in PHEM (60 mM PIPES, 25 mM HEPES, 10 mM EGTA, 2 mM $MgCl_2$, pH 6.9) containing 4% paraformaldehyde (PFA) (Electron Microscopy Sciences) for 20 minutes. Cells were washed extensively in PBS followed by permeabilization in PBS/0.5% Triton X-100 for 10 minutes. After several PBS washes, cells were processed for PLA according to (47) and manufacturer's instructions using the Orange detection kit with anti-mouse and anti-rabbit reagents (OLink/Sigma-Aldrich). Mouse anti-RIIα mAb (BD clone 40) and rabbit anti-PKAc (SCBT sc-903) were used to detect PKA holoenzymes. Z-stacks of fluorescent images were collected using a Leica DMI6000B inverted microscope with a spinning disk confocal head (Yokagawa) and a CoolSnap HQ camera (Photometrics) controlled by MetaMorph 7.6.4 (Molecular Devices). Maximum intensity projections were quantified for puncta number using Fiji/ImageJ. Images were smoothened and a duplicate image was created for use as a mask. The duplicate file was thresholded to capture as many puncta as possible without significant blending of densely packed signal. The binary mask was then used to measure selected regions from the original image. Total cell number per field of view was counted as DAPI-stained nuclei. Intensity profiles of raw images were produced in MetaMorph.

Live-cell FRET Imaging

HEK293 or U2OS cells were cultured on 35-mm glass coverslip dishes (MatTek Corporation) or 4-well glass bottom coverglass (ibidi). Cells were transiently transfected with cDNAs encoding different reporters alone, or together with either R2C2 fusion constructs or cDNAs encoding individual RII and C subunits. 24-48 hr after transfection, the cells were starved for 1 hour and then imaged in HEPES-Buffered Saline Solution (HBSS; 116 mM NaCl, 20 mM HEPES, 11 mM Glucose, 5 mM $NaHCO_3$, 4.7 mM KCl, 2.5 mM $CaCl_2$, 1.2 mM $MgSO_4$, 1.2 mM KH_2PO_4, pH 7.4). All imaging was performed at ambient temperature (25 - 28^{o}C). Cells were stimulated as indicated in individual figures. Fluorescence emission was acquired using a DMI6000B inverted microscope (Leica), an EL6000 component (fluorescent light source, filter wheel, ultrafast shutter; Leica) and a CoolSnap HQ camera (Photometrics), all controlled by MetaMorph 7.6.4 (Molecular Devices). Dual-emission images were obtained simultaneously through a DualView image splitter (Photometrics) with S470/30 and S535/30 emission filters and 505 dcxr dichroic mirror (Chroma). Exposure times were 100-500 ms. FRET changes within regions of interest were calculated as the ratio of measured fluorescent intensities from two channels (M_{donor}, $M_{indirectAcceptor}$) after subtraction of background signal. FRET ratio (YFP/CFP) changes were normalized to the average FRET ratio value before stimulation.

CREB Phosphorylation and Immunofluorescence

U2OS$^{R2A/R2B/CA}$ cells were plated onto poly-L-lysine coated coverslips and transfected with constructs encoding WT or M120A PKA-R2C2 fusion proteins as above. After 36 hours, cells were starved for 1 hour in serum free DMEM-H (ThermoFisher). Cells were then treated with indicated compounds for 30 minutes at 37^{o}C. Treated cells were rinsed in ice cold PBS and fixed in PBS containing 4% PFA. Cells were washed extensively in PBS, permeabilized for 10 minutes in PBS containing 0.5% Triton X-100 and 0.2% BSA and then washed several times in PBS. Cells were stained with anti-phospho-CREB serine 133 (Cell Signaling Technology (87G3); 1:500) overnight at 4^{o}C. Cells were washed in PBS and incubated with Alexa-488 conjugated secondary antibodies (ThermoFisher; 1:400) for 1 hour at room temperature. The cells were washed again in PBS twice and then incubated for 20 minutes with a 1:500 dilution of Texas Red-phalloidin (ThermoFisher) and DAPI. After final washing in PBS and a distilled H_2O rinse, coverslips were mounted in Prolong Diamond mounting media (ThermoFisher). Confocal microscopy was performed on a Zeiss LSM-510META laser scanning confocal microscope equipped with a Zeiss 63X, 1.4 numerical aperture, oil immersion objective. Z-stacks were collected and processed for max intensity projections using the Zen 2009 control software. Laser power, scan area and pinhole were kept constant across all conditions. Further image processing was performed in Fiji/ImageJ. Fluorescent intensity was quantified by measuring an ROI encompassing the nucleus and a non-stained region for background (after importing and splitting channels using the BioFormats package). Corrected total nuclear fluorescence was calculated according to the following formula: CTNF = Integrated Density – (Area of selected nucleus * Mean fluorescence of background selection).

Bad Phosphorylation by Immunoblot

U2OS$^{R2A/R2B/CA}$ cells were plated in 6-well dishes and co-transfected with constructs encoding WT or M120A PKA-R2C2 fusion proteins and pEBG-mBad (Cell Signaling Technology; 100-250 ng/well). After ~36 hours, cells were starved for 1 hour in serum free DMEM-H (ThermoFisher). Cells were preincubated for 5 min at 37°C with DMSO or 2 μM 1-NM-PP1, followed by addition of 1 μM iso for a further 5 min at 37°C. Cells were lysed in 25 mM HEPES, pH 7.4, 150 mM NaCl, 1 mM EDTA, 1 mM EGTA, 20 mM NaF, 2% glycerol, 1% Triton X-100, 0.5% deoxycholate plus 100 nM okadaic acid and protease inhibitors. After cell debris removal by centrifugation, protein content of lysates was quantified using the BCA assay (ThermoFisher) in a 96-well plate. Equivalent amounts of total lysate (12-15 μg/lane) was separated on Bolt gradient gels (ThermoFisher) and transferred to nitrocellulose. Membranes were incubated with primary antibodies overnight at 4°C in TBST/Blotto. Prior to re-probing, membranes were stripped with 1X Re-Blot Plus Strong (Millipore) for 15 minutes and then re-blocked in Blotto. The following antibodies were used: phospho-Bad ser155 (Santa Cruz Biotechnology sc-101641), 1:1000; PKA-C mAb (BD clone 5B), 1:1000; GST (Santa Santa Cruz Biotechnology sc-459), 1:1000; GST-HRP (GenScript), 1:1000); GAPDH (Santa Cruz Biotechnology sc-25778), 1:1000. The membranes were washed extensively in TBST, incubated with HRP-labeled secondary antibodies (Jackson Immunoresearch), washed as before and developed using ECL (ThermoFisher) on an Alpha Innotech MultiImage III with FluoroChem Q software. Quantification using densitometry of pSer155 Bad signal was performed using Fiji/ImageJ and normalized to corresponding GST immunoblot signal (for total Bad).

Apoptosis Assay using Fluorescent DEVD Substrate

U2OS$^{R2A/R2B/CA}$ cells were transfected with constructs encoding WT or M120A PKA-R2C2 fusion proteins. Cells were re-plated onto poly-L-lysine coated 8-well chambered coverslips (ibidi) and incubated overnight in vehicle or 50μM etoposide (SCBT). Isoproterenol (1 μM) and the long-acting β-agonist formoterol (1 μM) (an attempt to keep β-AR-PKA signaling high during the time course of the overnight treatment) were also added to appropriate wells. After 16 hours, CellEvent™ Caspase-3/7 Green Detection Reagent (ThermoFisher) was added to cells at a final concentration of 2 μM for 1 hour at 37°C. Cells were fixed by direct addition of PFA (16%, Electron Microscopy Sciences) to 4% for 5 minutes. Media was then replaced with PBS containing 4% PFA for another 10 minutes. Cells were washed extensively in PBS, permeabilized for 10 minutes in PBS containing 0.5% Triton X-100 and 0.2% BSA and then washed several times in PBS. Cells were incubated with DAPI for 20 minutes and stored in PBS. For imaging, PBS was replaced with Vectashield (Vector Labs). Images were acquired on our Leica spinning-disk confocal microscope as described above.

Cell Growth Assay

U2OS$^{R2A/R2B/CA/CB}$ (R2C2-M120A stable, Cβ KO) cells were created as described above, using a sgRNA targeting PRKACB (sequence: 5'-CATGGCATAATACTGTTCAG-3'). Several clones with interruptions of the PRKACB gene were expanded and subjected to cell growth assays using the CellTiter 96® AQ_{ueous} One Solution cell proliferation assay (Promega, Madison, WI). Cells were plated in a 96-well plate in triplicate at 1000 cells per well in 100 μl. After 24 hours, 20 μl assay solution was added to each well and cells were grown another 3 hours at 37°C, 5% CO_2. Absorbance at 490 nm was read on a POLARstar Omega plate reader (BMG Labtech). Counts were background subtracted using wells containing only growth media.

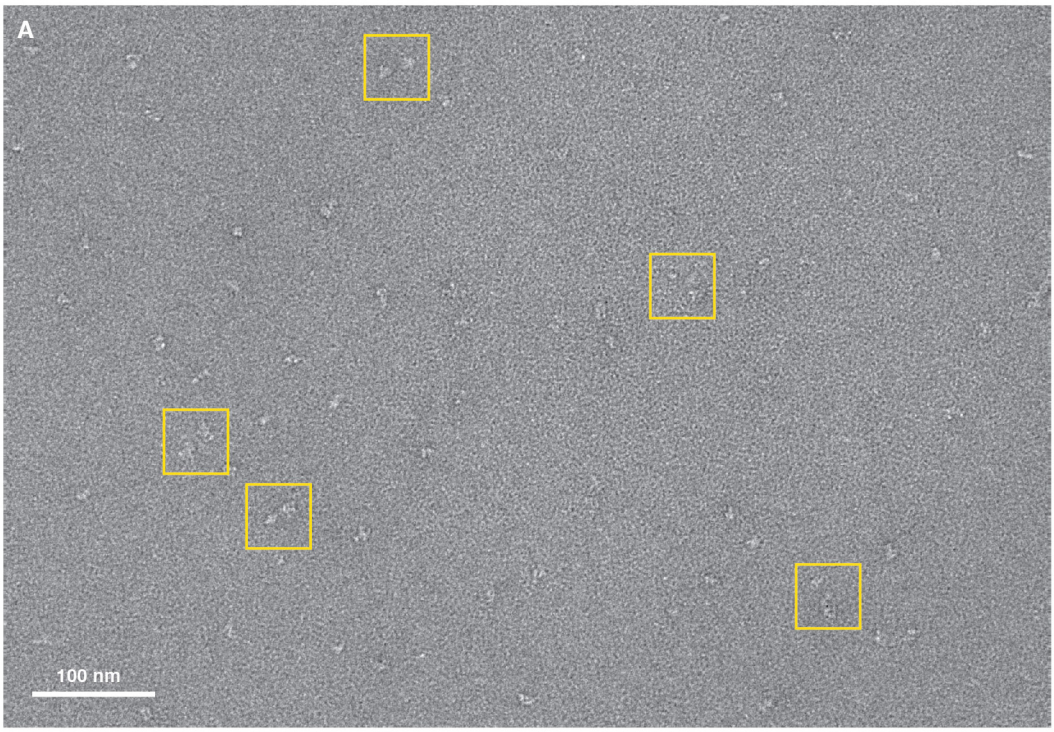
A
100 nm

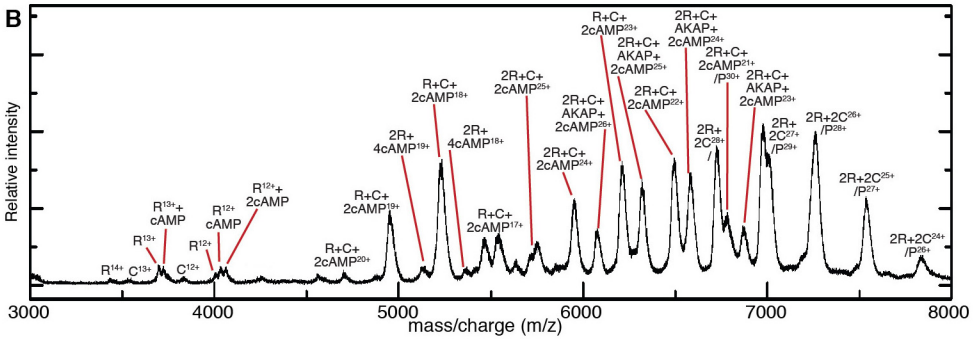
B
Relative intensity
mass/charge (m/z)
3000
4000
5000
6000
7000
8000
R14+ C13+
R13+
R13+ + cAMP
C12+
R12+
R12+ cAMP
R12+ + 2cAMP
R+C+ 2cAMP20+
R+C+ 2cAMP19+
2R+ 4cAMP19+
R+C+ 2cAMP18+
2R+ 4cAMP18+
R+C+ 2cAMP17+
2R+C+ 2cAMP25+
2R+C+ 2cAMP24+
R+C+ 2cAMP23+
2R+C+ AKAP+ 2cAMP26+
2R+C+ AKAP+ 2cAMP25+
2R+C+ 2cAMP22+
2R+C+ AKAP+ 2cAMP24+
2R+ 2C28+
2R+C+ 2cAMP21+ /P30+
2R+C+ AKAP+ 2cAMP23+
2R+ 2C27+ /P29+
2R+2C26+ /P28+
2R+2C25+ /P27+
2R+2C24+ /P26+

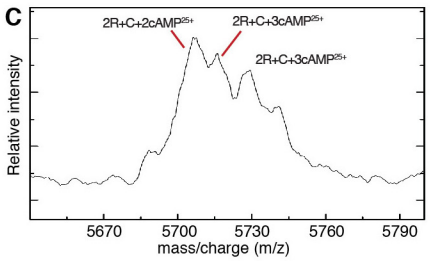
C
Relative intensity
mass/charge (m/z)
5670
5700
5730
5760
5790
2R+C+2cAMP25+
2R+C+3cAMP25+
2R+C+3cAMP25+

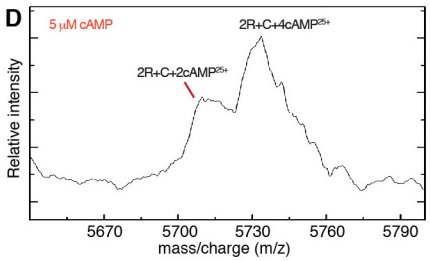
D
5 μM cAMP
Relative intensity
mass/charge (m/z)
5670
5700
5730
5760
5790
2R+C+2cAMP25+
2R+C+4cAMP25+

Fig. S1.

Additional data related to figure 1. **(A)** Raw EM micrograph of AKAP79-PKA holoenzyme complexes. Purified proteins were assembled into complexes and processed by the GraFix method (43). Dilute samples were applied to carbon coated grids and negative-stained with uranyl formate. Grids were imaged on a Tecnai T12 TEM at 0.7-1.5 micron defocus ranges. Representative particles picked for further analysis are boxed (yellow squares). **(B)** Native nESI mass spectrum of RII+C+AKAP$^{297\text{-}427}$ complexes. Indicated are the charge states of each of the observed and annotated molecular ions (see associated tables S1 and S2). Data were acquired on the Synapt G2-S*i* (Waters). **(C)** Native nESI mass spectrum of RII+C complexes without additional cAMP. The 25+ charge state of the 2RII:C:**n**cAMP complexes are presented (see associated table S3). Data were acquired on the Exactive™ Plus EMR Orbitrap (ThermoScientific). **(D)** Native nESI mass spectrum of RII+C complexes with additional cAMP (5 µM; RII:C:cAMP ratio of 1:1:2). The 25+ charge state of the 2RII:C:**n**cAMP complexes are presented (see associated table S3). Data were acquired on the Exactive™ Plus EMR Orbitrap (ThermoScientific).

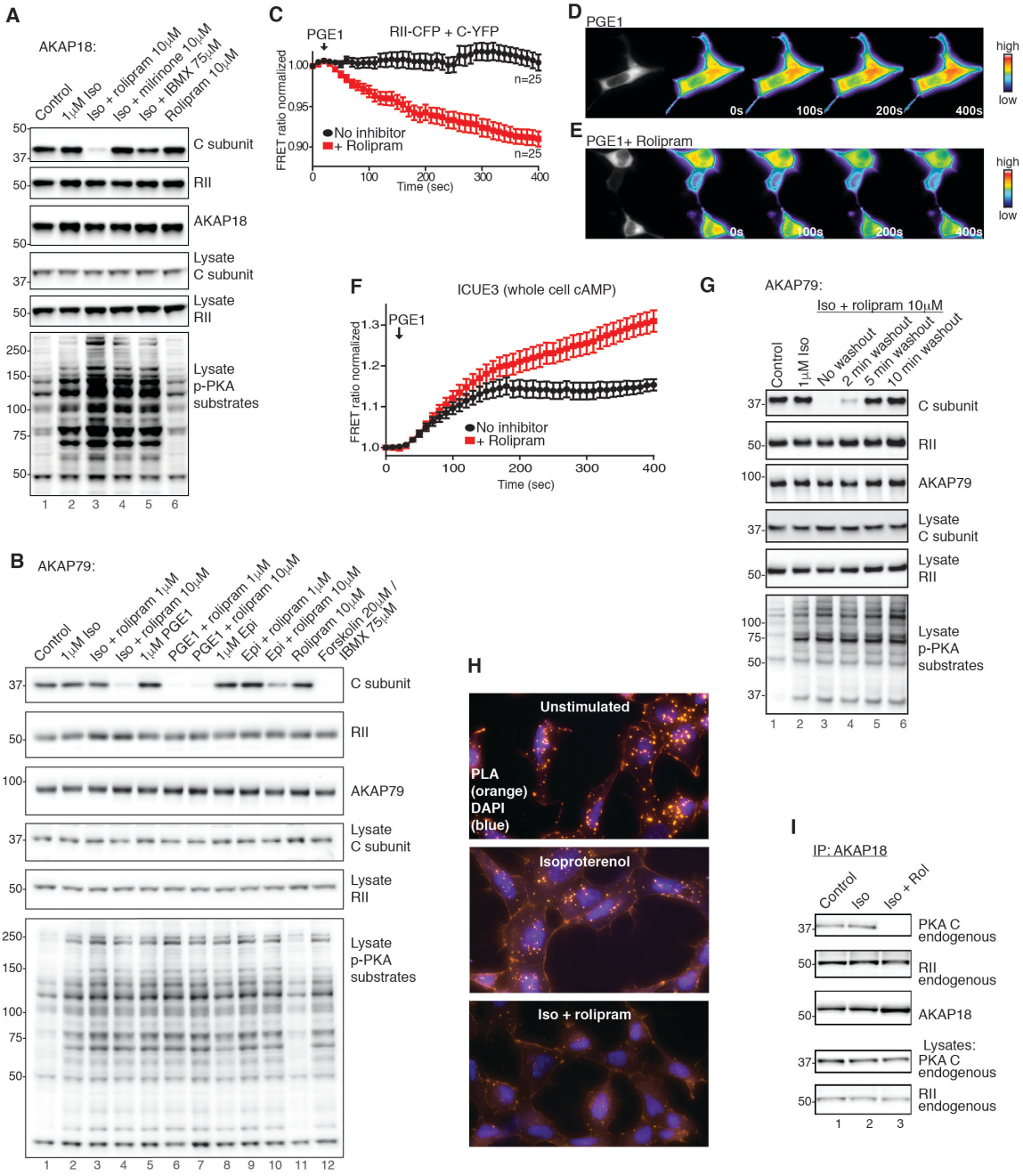

Fig. S2

Additional data related to figure 2. *Anchored PKA holoenzymes remain associated during submaximal cAMP pulses and can re-form quickly upon removal of supraphysiological stimuli.* **(A)** HEK293 cells expressing AKAP18γ-GFP and RIIa-V5 were stimulated for 5 minutes with 1 μM isoproterenol alone or after 5-minute pre-incubation with PDE inhibitors as indicated. AKAP18γ was immunoprecipitated, and immune complexes and lysates were probed for

associated PKA subunits by Western blotting. Detection of phosphorylated PKA substrates was used to confirm activation of PKA signaling. **(B)** HEK293 cells expressing AKAP79-GFP and RIIα-V5 were stimulated for 5 minutes with indicated compounds alone or after 5-minute pre-incubation with PDE inhibitors as above. Forskolin/IBMX treatment was for 20 minutes. AKAP79 was immunoprecipitated and immune complexes and lysates were probed for associated PKA subunits by Western blotting. Detection of phosphorylated PKA substrates was used to confirm activation of PKA signaling. **(C)** FRET recordings in HEK293 cells expressing the paired RII-CFP/PKAc-YFP biosensor upon PGE_1 stimulation in the presence (red) or absence (black) of rolipram. **(D)** Representative images from PGE_1 treated cells. **(E)** Representative images from PGE1 + rolipram treated cells. **(F)** FRET recordings in HEK293 cells expressing the ICUE3 cAMP biosensor upon PGE_1 stimulation in the presence (red) or absence (black) of rolipram. **(G)** HEK293 cells expressing AKAP79-GFP and RIIα-V5 were stimulated for 5 minutes with 1 μM isoproterenol or were stimulated with iso + rolipram followed by a washout period of different lengths in which drug was removed and replaced with fresh serum-free DMEM. AKAP79 was then immunoprecipitated, and immune complexes and lysates were probed for associated PKA subunits. Detection of phosphorylated PKA substrates was used to confirm activation of PKA signaling. **(H)** HEK293 cells on glass coverslips were stimulated as described above and then fixed in 4% PFA for proximity ligation assays. Cells were processed for detection of the interaction between RII and C with the Orange PLA detection kit (Sigma-Aldrich) and co-stained for DAPI to detect nuclei. **(I)** HEK293 cells expressing AKAP18γ-GFP were stimulated for 5 minutes with 1 μM isoproterenol alone or after 5-minute pre-incubation with rolipram (10 μM). AKAP18γ was immunoprecipitated, and immune complexes and lysates were probed for associated PKA subunits by Western blotting.

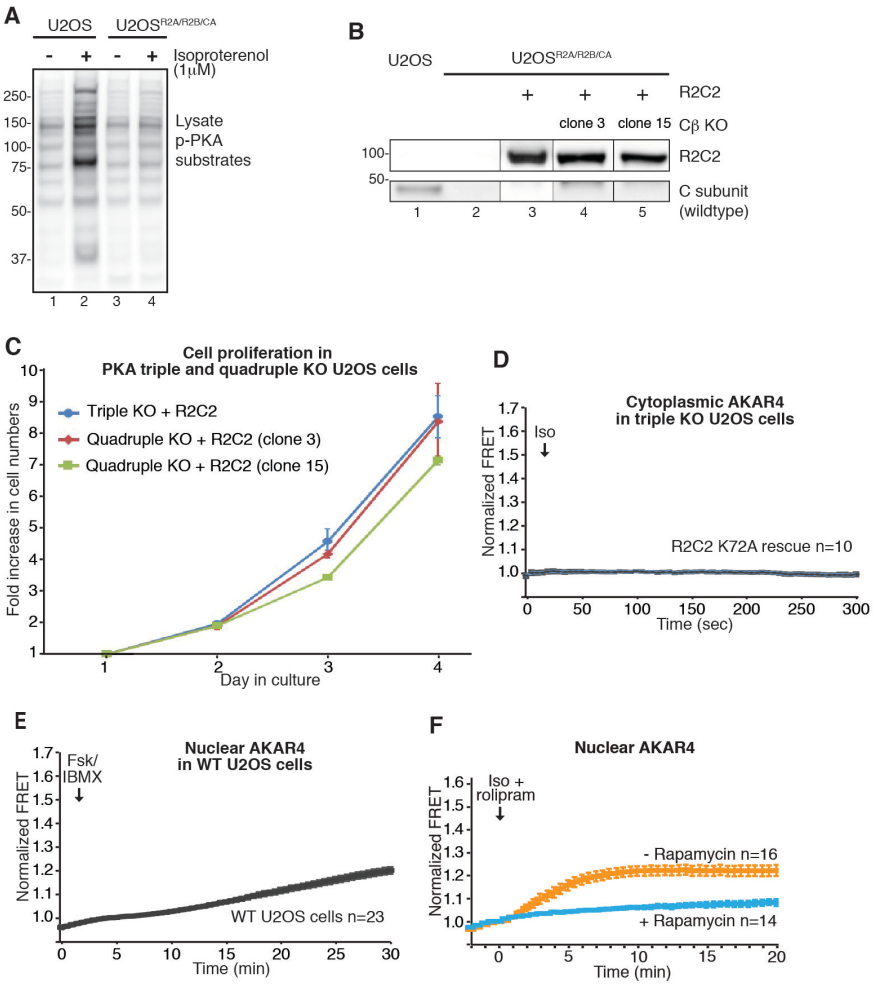

Fig. S3

Additional data related to figure 3. **(A)** Immunoblotting using phospho-PKA substrates antibodies of cell lysates from wild-type U2OS and U2OS$^{R2A/R2B/CA}$ cells after treatment with isoproterenol (1 μM, 5 min). **(B)** Immunoblotting of wild-type U2OS, U2OS$^{R2A/R2B/CA}$, U2OS$^{R2A/R2B/CA}$-R2C2 stable, and two clonal lines of U2OS$^{R2A/R2B/CA/CB}$-R2C2 stable (Cβ KO) cells with antibodies against PKA C-subunit. These blots were assembled from two different experiments to demonstrate stable expression of the R2C2 fusion protein. **(C)** MTS assay on triple knockout cells stably expressing R2C2-M120A and two clones of quadruple knockout lines derived from these cells. **(D)** AKAR4^{NES} cytoplasmic FRET recordings in Iso-stimulated U2OS$^{R2A/R2B/CA}$ cells expressing "kinase-dead" R2C2 K72A. **(E)** AKAR4^{NLS} nuclear FRET recordings in wild-type U2OS cells in response to forskolin/IBMX treatment. **(F)** AKAR4^{NLS} nuclear FRET recordings in U2OS$^{R2A/R2B/CA}$ cells expressing FKBP-RII and FRB-C in response to stimulation with isoproterenol and rolipram (1 μM/10 μM), in the absence (orange) or presence (blue) of rapamycin (100 nM).

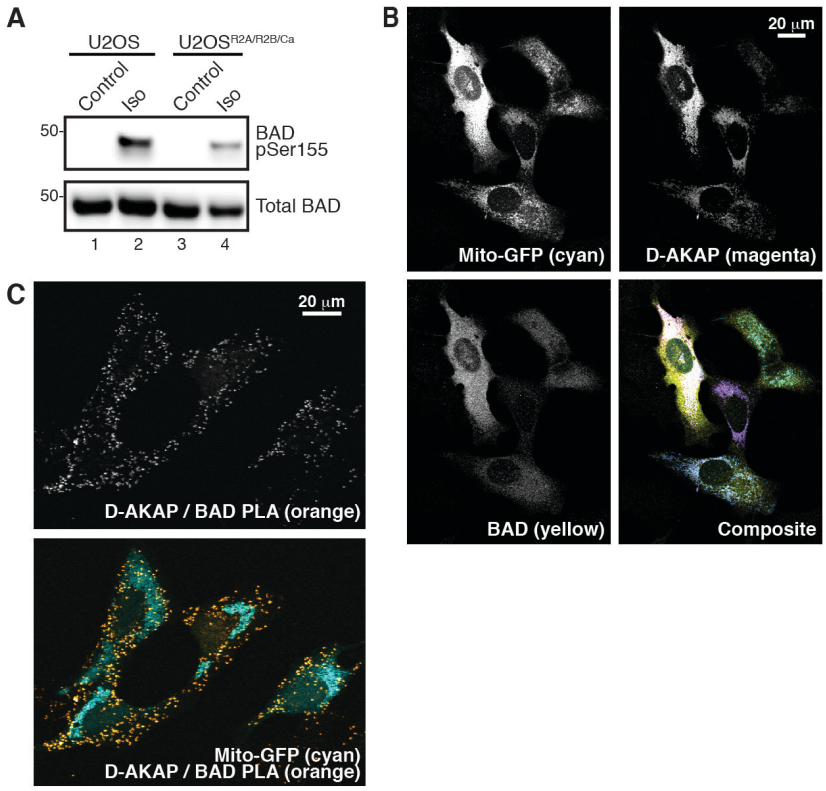

Fig. S4

Additional data related to figure 4. **(A)** Wild-type U2OS and U2OS$^{R2A/R2B/CA}$ were transfected with a plasmid encoding GST-BAD. Cells were treated with isoproterenol (1 μM) or vehicle for 5 minutes. Immunoblot detecting BAD pSer155 and total BAD (GST). **(B)** U2OS$^{R2A/R2B/CA}$ transiently expressing mitochondrially-targeted GFP, D-AKAP-1 and GST-BAD were fixed, stained and imaged using confocal microscopy. **(C)** U2OS$^{R2A/R2B/CA}$ transiently expressing mitochondrially-targeted GFP, D-AKAP-1 and GST-BAD were fixed, processed for proximity ligation and imaged using confocal microscopy. Fluorescence is shown in grayscale except for composite images.

Table S1: Theoretical and observed *m/z* values for each of the observed complexes of RII, C, AKAP79$^{297-427}$ with or without cAMP as measured by native MS. Data were acquired on the Synapt G2-S*i* (Waters).

Complex	Charge state	[a] *m/z* theoretical	*m/z* observed	[b] delta
C	12	3834.9	3834.4	-0.5
	13	3540.0	3535.1	-4.9
RII	12	4006.3	4004.7	-1.6
	13	3698.2	3699.4	1.2
	14	3434.1	3433.4	-0.7
RII:cAMP	12	4033.8	4034.0	0.2
	13	3723.6	3723.9	0.3
RII:2cAMP	12	4061.2	4061.4	0.2
	13	3748.9	3747.9	-1.0
2RII:4cAMP	18	5414.6	5419.3	4.7
	19	5129.7	5130.7	1.0
RII:C	17	5534.6	5540.6	6.0
	18	5227.2	5228.5	1.3
	19	4952.1	4951.7	-0.4
	20	4704.6	4704.2	-0.4
2RII:C:2cAMP	22	6491.6	6497.4	5.8
	23	6209.4	6213.7	4.3
	24	5950.7	5952.5	1.8
	25	5712.7	5717.7	5.0
2RII:2C	24	7840.3	7834.7	-5.6
	25	7526.7	7538.3	11.6
	26	7237.2	7260.4	23.2
	27	6969.2	6977.7	8.5
2RII:C:AKAP:2cAMP	23	6868.4	6872.0	3.6
	24	6582.2	6582.5	0.3
	25	6319.0	6320.3	1.3
	26	6076.0	6077.7	1.7
2RII:2C:AKAP (P)	26	7820.2	7834.7	14.5
	27	7530.6	7538.3	7.7
	28	7261.6	7260.4	-1.2
	29	7011.3	7006.1	-5.2
	30	6777.6	6782.0	4.4

[a] Theoretical masses (and *m/z* values) of the complexes were calculated using the native experimental mass data for the individual subunits under the same experimental conditions.

[b] Difference between theoretical and observed values arise due to incomplete desolvation and adducts of Na^+ that are typical of these types of native mass spectrometry analyses.

Table S2: Theoretical and experimentally computed masses (Da) of each of the observed complexes of RII, C, AKAP79$^{297-427}$ with or without cAMP following native MS (Supplementary Table 1; Fig 1). Data were acquired on the Synapt G2-S*i* (Waters).

Complex	[a]Theoretical mass (Da)	Experimental mass (Da)	[b]Delta mass (Da)
R:C	94,071	94,000	71
2R:C:2cAMP	142,793	142,600	193
2R:C:AKAP:2cAMP	157,949	157,800	149
2R:2C	188,142	188,100	42
2R:2C:AKAP	203,298	203,200	98

[a] Theoretical masses of the complexes were calculated using the native experimental mass data for the individual subunits under the same experimental conditions.

[b] It should be noted that the difference between theoretical and observed values arise largely due to incomplete desolvation and adducts of Na^+ that are typical of these types of native mass spectrometry analyses. Consideration should also be given to the multiple phosphorylated forms of the catalytic subunit C, given that an average of 7 (5 – 10) phosphate molecules are typically observed for heterologously expressed catalytic enzyme (Ref. 10).

Supplementary Table 3: Theoretical and observed *m/z* values for the 25+ charge state of the 2RII:C:ncAMP complexes, without or with additional cAMP (5 µM; RII:C:cAMP ratio of 1:1:2), as measured by native MS. Data were acquired on the Exactive™ Plus EMR Orbitrap (ThermoScientific).

RII:C:cAMP Ratio	Complex	Charge state	[a] *m/z* theoretical	*m/z* observed	[b] delta
1:1:0	**2RII:C:2cAMP**	25	5706.1	5706.6	0.5
	2RII:C:3cAMP	25	5719.3	5715.8	-3.5
	2RII:C:4cAMP	25	5732.4	5728.4	-4.0
1:1:2	**2RII:C:2cAMP**	25	5706.1	5712.8	6.7
	2RII:C:4cAMP	25	5732.4	5732.8	0.4

[a] Theoretical masses (and m/z values) of the complexes were calculated using the native experimental mass data for the individual subunits under the same experimental conditions.

[b] Difference between theoretical and observed values arise due to incomplete desolvation and adducts of Na^+ that are typical of these types of native mass spectrometry analyses.